ISSN 1615-9306 · JSSCCJ 44 (14) 2021 · Vol. 44 · No. 14 · July 2021

Journal of SEPARATION SCIENCE

14|2021

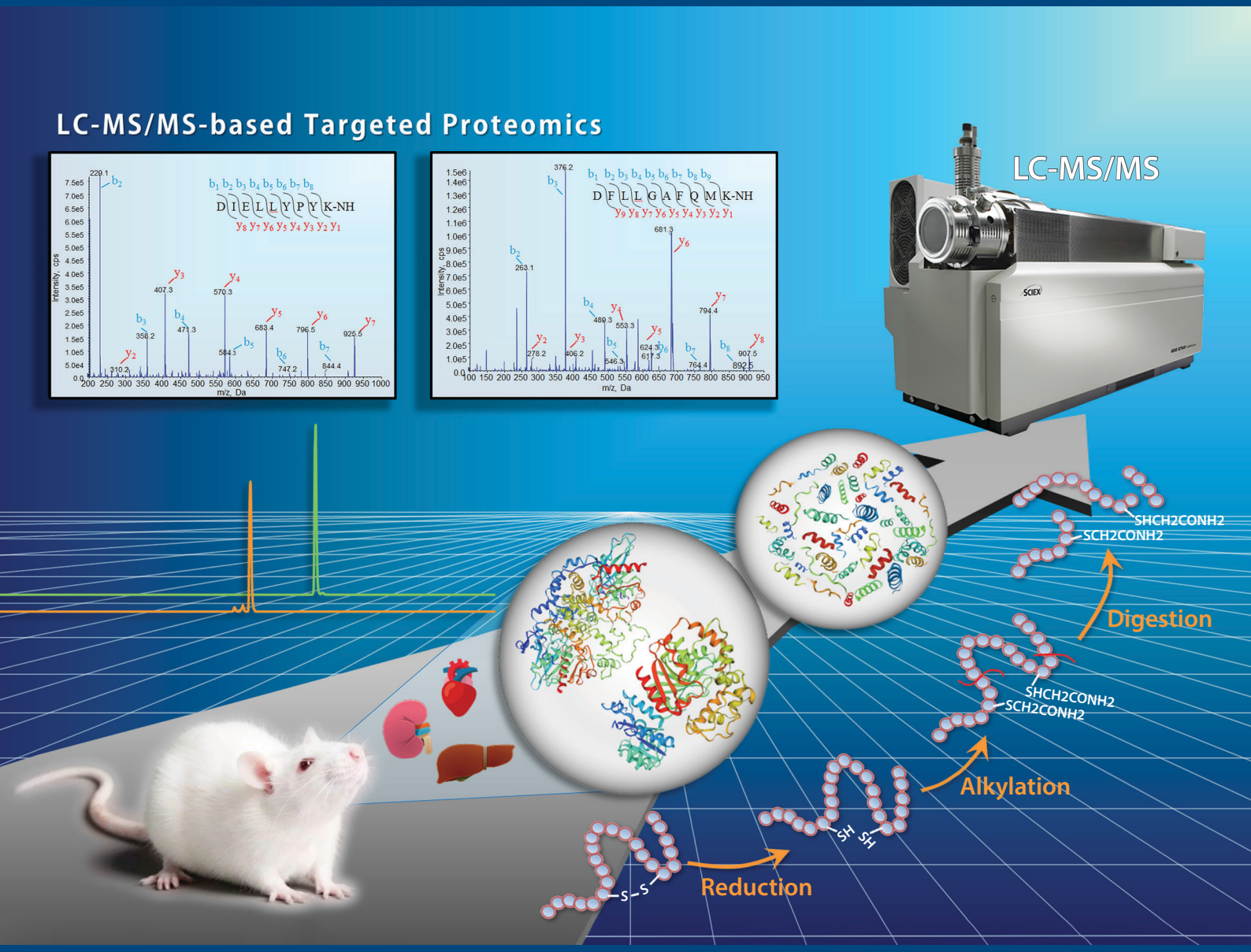

Methods
Chromatography · Electroseparation

Applications
Biomedicine · Foods · Environment

www.jss-journal.com

WILEY-VCH

Received: 10 March 2021 | Revised: 28 April 2021 | Accepted: 29 April 2021

DOI: 10.1002/jssc.202100201

JOURNAL OF SEPARATION SCIENCE

RESEARCH ARTICLE

Plate-height model of ion mobility-mass spectrometry: Part 2—Peak-to-peak resolution and peak capacity

Márkó Grabarics[1,2] | **Maike Lettow**[1,2] | **Ansgar T. Kirk**[3] | **Gert von Helden**[2] | **Tim J. Causon**[4] | **Kevin Pagel**[1,2]

[1] Institute of Chemistry and Biochemistry, Freie Universität Berlin, Berlin, Germany

[2] Department of Molecular Physics, Fritz Haber Institute of the Max Planck Society, Berlin, Germany

[3] Institute of Electrical Engineering and Measurement Technology, Leibniz Universität Hannover, Hannover, Germany

[4] Institute of Analytical Chemistry, University of Natural Resources and Life Sciences, Vienna, Austria

Correspondence
Márkó Grabarics, Institute of Chemistry and Biochemistry, Freie Universität Berlin, Arnimallee 22, 14195, Berlin, Germany.
Email: grabarics@fhi-berlin.mpg.de

Funding information
Freie Universität Berlin and the Max Planck Society; German Research Foundation, Grant/Award Number: PA 1766/3-1

In a previous work, we explored zone broadening and the achievable plate numbers in linear drift tube ion mobility-mass spectrometry through developing a plate-height model [1]. On the basis of these findings, the present theoretical study extends the model by exploring peak-to-peak resolution and peak capacity in ion mobility separations. The first part provides a critical overview of chromatography-influenced resolution equations, including refinement of existing formulae. Furthermore, we present exact resolution equations for drift tube ion mobility spectrometry based on first principles. Upon implementing simple modifications, these exact formulae could be readily extended to traveling wave ion mobility separations and to cases when ion mobility spectrometry is coupled to mass spectrometry. The second part focuses on peak capacity. The well-known assumptions of constant plate number and constant peak width form the basis of existing approximate solutions. To overcome their limitations, an exact peak capacity equation is derived for drift tube ion mobility spectrometry. This exact solution is rooted in a suitable physical model of peak broadening, accounting for the finite injection pulse and subsequent diffusional spreading. By borrowing concepts from the theoretical toolbox of chromatography, we believe that the present study will help in integrating ion mobility spectrometry into the unified language of separation science.

KEYWORDS
drift tube, ion mobility spectrometry, peak capacity, peak resolution, traveling wave

1 | INTRODUCTION

In recent years, ion mobility spectrometry (IMS), both as a stand-alone technique and in combination with MS (IM-MS), has been the subject of intense research. These efforts led to remarkable improvements in the sensitivity, versatility, and resolving power of commercial and custom-built instruments [2]. Among the many creative ways invented to harness electric forces for separating ions in gases, drift tube (DT)IMS, traveling wave (TW)IMS, trapped (T)IMS and field asymmetric waveform (FA)IMS proved to be the most successful [3,4]. The primary focus of the present study is DTIMS and DTIM-MS within the low-field limit. However, similarities between DTIMS and TWIMS allow

Article Related Abbreviations: DTIMS, drift tube ion mobility spectrometry; IM-MS, ion mobility-MS; TWIMS, traveling wave ion mobility spectrometry; VMD, virtual migration distance

for occasional extension of the plate-height model to derive equations applicable for the latter technique as well.

DTIMS is a gas-phase electrophoretic method, where charged analytes are separated according to their mobilities (K) as they drift through a gas-filled cell, propelled by a static, homogeneous electric field [5]. Mobilities are related to the mass, charge, size, and shape of ions, whereby the motion of ions is governed by two-body collisions with the neutral gas particles [6,7]. Within the low-field limit, these collisions are essentially thermal (low reduced field-strengths), making mobilities virtually independent of the applied drift voltage. In general, nonlinear effects on zone broadening are weak, and peaks converge to a Gaussian profile. Thus, plate-height models can be efficiently applied to describe DTIM separations. Having explored zone dispersion in detail previously [1], in the present study we further extend the plate-height model of IM-MS and derive suitable formulae for peak-to-peak resolution and peak capacity.

Single-peak resolving power (R_P), the number of theoretical plates (N), and the plate height (HETP) are highly useful indices to characterize and compare the performance of separation methods based on differential migration. However, the analyst facing a practical problem is often more interested in the actual resolution between two neighboring peaks. Peak-to-peak resolution (R_S) is a widely employed, dimensionless measure of the extent of separation between two Gaussian peaks [8]:

$$R_S = \frac{t_2 - t_1}{2\sigma_{t,1} + 2\sigma_{t,2}} = \frac{|\Delta t|}{4\langle\sigma_t\rangle} \tag{1}$$

In Equation (1), t_1 and t_2 are the centroid drift times (or retention times, migration times, etc.), while $\sigma_{t,1}$ and $\sigma_{t,2}$ are the corresponding temporal SDs of the distributions. By employing the absolute drift time (or retention time, migration time) difference $|\Delta t|$ and the arithmetic mean of the standard deviations $\langle\sigma_t\rangle$, a more concise formulation ensues. Despite the apparent similarity of the two phrases appearing in IMS literature, single-peak resolving power R_P and peak-to-peak resolution R_S should not be confused. The first is related to the sharpness of a single selected signal in the IM spectrum, often defined in a collision cross-section domain [2]. In contrast, R_S reflects separation between two adjacent peaks, influenced by both the width of the two signals as well as the distance between them.

The rationale behind Equation (1) is as follows: considering two identical Gaussians with the same area and SD, R_S will be unity when the line tangents to the closer-lying inflection points of the peaks intersect at the baseline. Unit resolution ($R_S = 1$) in these cases means that each peak overlaps 4.55% of the other peak's area, while baseline resolution ($R_S = 1.5$) results in a 0.27% overlap. The above values, however, change at constant R_S if the two peaks are not identical: the same R_S value may apply to different peak pairs with different overlap, depending on the ratio of their areas and SDs. Thus, R_S is not a direct measure of cross-contamination, and alternative functions were developed that are better suited for preparative separations and non-Gaussian peak profiles [9–11]. Although many of these functions reflect peak overlap more accurately, they are much more difficult to calculate from experimental data and have no clear advantages over Equation (1) in analytical separations, impeding their widespread application. Thus, in separation science, Equation (1) serves as a practical and universally recommended index for measuring resolution between peaks. Owing to its simplicity, popularity, direct connection to peak capacity (see later) and the fact that it served as the starting point for predictive resolution equations in chromatography and electrophoresis, we also choose Equation (1) as the basic definition to derive predictive formulae for stand-alone IMS and IM-MS.

2 | RESULTS AND DISCUSSION

2.1 | Chromatography-influenced predictive resolution equations for drift tube ion mobility spectrometry

Being a general definition and entirely descriptive, Equation (1) merely specifies the way resolution should be calculated in case an ion mobility spectrum, chromatogram, etc., is given. However, it does not help us identify underlying factors influencing resolution, nor does it help to find the optimal separation conditions. Therefore, predictive equations need to be derived that reveal the fundamental factors determining R_S, aid the optimization of separations in practice, and may estimate R_S under prescribed experimental conditions. For clarity, in resolution equations specific for a certain technique the respective separation method is indicated in the subscript of R_S.

2.1.1 | Equal peak width assumption

Assuming $\sigma_{t,1} + \sigma_{t,2} = 2\sigma_{t,2}$, Purnell derived a predictive resolution equation for column chromatography under linear elution conditions [12]:

$$R_{S,\,Ch} = \frac{\sqrt{N_2}}{4}\frac{k_2 - k_1}{1 + k_2} = \frac{\sqrt{N_2}}{4}\frac{\alpha - 1}{\alpha}\frac{k_2}{1 + k_2} \tag{2}$$

In Equation (2), N_2 is the plate number for the later eluting component, and k_1 and k_2 are the retention factors of

the respective compounds, while α is the separation factor expressing intrinsic selectivity ($\alpha = k_2/k_1$). The subscript in $R_{S,Ch}$ refers to chromatography. Definitions of chromatographic parameters appearing seldom in the IMS literature are provided in the Supporting Information, Section S1.

Employing the same equal peak width assumption, but concentrating on the first peak ($\sigma_{t,1} + \sigma_{t,2} = 2\sigma_{t,1}$), Knox [13] and Thijssen [14] arrived at the following formula:

$$R_{S,Ch} = \frac{\sqrt{N_1}}{4}\frac{|\Delta k|}{1+k_1} = \frac{\sqrt{N_1}}{4}(\alpha - 1)\frac{k_1}{1+k_1} \quad (3)$$

Here, N_1 is the plate count for the earlier eluting solute and $|\Delta k|$ stands for the absolute difference of retention factors.

Equations (2) and (3) are equivalent and yield the same result as Equation (1), provided the assumption of equal peak widths is satisfied ($\sqrt{N_1}(1+k_2) = \sqrt{N_2}\,(1+k_1)$). This criterion, however, is often not met in practice, in which case Equations (2) and (3) cease to be equivalent and the choice to apply one or the other becomes arbitrary. If the second peak is broader, as in most cases, R_S values predicted by Equation (2) will be systematically lower, while those predicted by Equation (3) will be systematically higher than the reference values calculated according to Equation (1). Detailed derivations of the resolution equations presented in Sections 2.1–2.3 can be found in the Supporting Information, Section S2.

The first predictive resolution equation for DTIMS [15] was based on Equation (2), inheriting its limitations stemming from the equal peak width assumption:

$$R_{S,DT} = \frac{\sqrt{N_2}}{4}\frac{\alpha - 1}{\alpha} \quad (4)$$

Here, α is defined as the ratio of ion mobilities instead of the ratio of retention factors as in chromatography ($\alpha \geq 1$ by convention). The subscript in $R_{S,DT}$ indicates that Equation (4) is specific to DTIM separations.

The general reasoning to obtain Equation (4) is as follows: the time the ions need to traverse an empty drift cell in perfect vacuum (i.e., the analogue of chromatographic void time) is negligibly short compared to the actual drift time in gas-filled cells (equivalent of retention time). Therefore, retention factors in DTIMS are virtually infinite, meaning that the chromatographic migration factor $k_2/(1+k_2)$ is essentially unity and may be neglected. Although the resulting formula is useful, the above argument is not justified by physical models and may be misleading: it implies that IMS is a chromatography-like process with retention playing a central role. Instead, IMS is a gas-phase electrophoretic process where convective flow or partition between stationary and mobile phases are absent. Thus, void time and retention (factors) cannot be interpreted in relation to this technique.

To circumvent the shortcomings of the above reasoning that stem from physical differences between the techniques, we may instead concentrate on more abstract, general aspects of differential migration processes and utilize the concept of virtual migration distances (VMDs), developed by Rathore and Horváth [16]. VMDs reveal analogies between separation methods and the equivalence of separation parameters across techniques. In this system, the equivalent of the chromatographic migration factor is the electromigration factor, which in case of DTIMS—electrophoretic process in the absence of bulk flow—equals 1. The equivalent of the chromatographic retention factor is the electrophoretic velocity factor, which is infinitely large in DTIMS, analogously to condensed-phase zone electrophoresis without electroosmotic flow. Thus, obtaining Equation (4) from Equation (2) appears justified based on this concept. For the detailed description of VMDs, the interested reader is referred to the seminal publication [16]. The equivalent separation parameters mentioned above together with respective VMDs are summarized in the Supporting Information, Table S1.

2.1.2 | Equal plate number assumption and exact solutions

A generally more valid assumption for close-lying peaks in isocratic elution chromatography and DTIMS is that of equal plate numbers. Assuming $N_1 = N_2 = N$, Karger obtained the following equation for chromatography [17]:

$$R_{S,Ch} = \frac{\sqrt{N}}{4}\frac{|\Delta k|}{1+\langle k\rangle} = \frac{\sqrt{N}}{4}\left(2\frac{\alpha-1}{\alpha+1}\frac{\langle k\rangle}{1+\langle k\rangle}\right) \quad (5)$$

In Equation (5), $\langle k\rangle$ is the arithmetic mean of the retention factors.

An exact solution requiring no assumption on the width of peaks or the plate number was derived by Said [18,19] and Suematsu and Okamoto [20] by introducing an effective average plate number corresponding to a hypothetical analyte, defined as:

$$N_{avg} = \left(\frac{\langle t_R\rangle}{\langle \sigma_t\rangle}\right)^2 \quad (6)$$

Here, $\langle t_R\rangle$ is the arithmetic mean of the two retention times, while the denominator contains the arithmetic mean of the peaks' temporal SDs. In practice, the ratio of N_1 and N_2 is generally close to unity, in which case the arithmetic [19,21] or geometric mean [22] of the plate numbers serve as sufficiently good approximation for N_{avg}. The

TABLE 1 Corresponding predictive resolution equations for chromatography and drift tube ion mobility spectrometry

Chromatography	Drift tube ion mobility spectrometry	Assumption	Reference and name
$\frac{\sqrt{N_1}}{4}(\alpha-1)\frac{k_1}{1+k_1}$	$\frac{\sqrt{N_1}}{4}(\alpha-1)$	$\sigma_{t,1}+\sigma_{t,2}=2\sigma_{t,1}$	Knox-Thijssen [13,14]
$\frac{\sqrt{N_2}}{4}\frac{\alpha-1}{\alpha}\frac{k_2}{1+k_2}$	$\frac{\sqrt{N_2}}{4}\frac{\alpha-1}{\alpha}$	$\sigma_{t,1}+\sigma_{t,2}=2\sigma_{t,2}$	Purnell [12]
$\frac{\sqrt{N}}{4}\left(2\frac{\alpha-1}{\alpha+1}\frac{\langle k\rangle}{1+\langle k\rangle}\right)$	$\frac{\sqrt{N}}{2}\frac{\alpha-1}{\alpha+1}$	$N_1=N_2=N$	Karger [17]
$\frac{\sqrt{N_{avg}}}{4}\left(2\frac{\alpha-1}{\alpha+1}\frac{\langle k\rangle}{1+\langle k\rangle}\right)$	$\frac{\sqrt{N_{avg}}}{2}\frac{\alpha-1}{\alpha+1}$	No assumption (exact)[a]	Said [18–20]
$\frac{\sqrt{N_{geo}}}{4}\left(2\frac{\alpha-1}{\alpha+1}\frac{\langle k\rangle}{1+\langle k\rangle}\right)$	$\frac{\sqrt{N_{geo}}}{2}\frac{\alpha-1}{\alpha+1}$	Empirical[b]	–

[a] $N_{avg}=(\langle t\rangle/\langle\sigma_t\rangle)^2$, the effective average plate number.
[b] $N_{geo}=\sqrt{N_1N_2}$, that is, the geometric mean of the two plate numbers.

resulting exact predictive equation for R_S is very similar to Equation (5):

$$R_{S,Ch}=\frac{\sqrt{N_{avg}}}{4}\frac{|\Delta k|}{1+\langle k\rangle}=\frac{\sqrt{N_{avg}}}{4}\left(2\frac{\alpha-1}{\alpha+1}\frac{\langle k\rangle}{1+\langle k\rangle}\right) \tag{7}$$

The only difference is the presence of N_{avg}. The term in parenthesis reflects the relative velocity difference of the analytes.

Equation (7) reveals the influence of fundamental separation parameters on resolution, does not suffer from the shortcomings of Equations (2) and (3), and yields the same R_S values as Equation (1) in all cases, irrespective of the ratio of peak widths or plate numbers. Therefore, we may choose it as the basis of a more accurate formula for DTIMS:

$$R_{S,DT}=\frac{\sqrt{N_{avg}}}{2}\frac{\alpha-1}{\alpha+1} \tag{8}$$

Here, N_{avg} is calculated according to Equation (6), using drift times (t_D) instead of retention times. Inheriting the above-mentioned advantages of Equation (7), Equation (8) appears as a suitable choice for a predictive resolution equation in DTIMS. Table 1 provides a concise overview of resolution equations for chromatography along with the analogous formulae for IMS.

Figure 1 compares the performance of chromatography-influenced predictive resolution equations for DTIMS, highlighting their trueness under a broad range of settings. Figure 1a portrays the situation with equal plate numbers assumed for the two separands. R_S values predicted by equations based on the equal peak width assumption (red and yellow traces) show increasing deviation from the true R_S with growing values of α, that is, as the distance between the peaks in the ion mobility spectrum increases. Although the experimentally most relevant region is that of close-lying peaks where α is relatively low, the results clearly indicate the limitations of the equal peak width assumption. Figure 1b represents a different setting: the ratio of the two peaks' temporal width is swept between 1 and 1.5, while α is held constant at 1.05. As the second peak becomes broader relative to the first, equations based on various assumptions show increasing systematic deviation. Meanwhile, the exact equation (based on Said's formula for chromatography) successfully predicts the true value of R_S in the entire range. The empirical formula, where N_{avg} is approximated by the geometric mean of the two plate numbers, yields results sufficiently close to the true value. Thus, it proves to be a good alternative in practice. It is worth mentioning that the green trace reproduces the true value at exactly one point: Where the peak width ratio equals the value $\alpha=1.05$. At this point, N_1 equals N_2 and the assumption the equation is based on is satisfied.

2.2 | Resolution equations for drift tube ion mobility spectrometry from first principles

Starting from Equation (1), it can be shown that R_S depends on the number of theoretical plates and the relative velocity difference (δ_v, nonnegative by definition) of the analytes [23]:

$$R_S=\frac{|\Delta t|}{4\langle\sigma_t\rangle}=\frac{\sqrt{N_{avg}}}{4}\frac{|\Delta t|}{\langle t\rangle}=\frac{\sqrt{N_{avg}}}{4}\frac{|\Delta v|}{\langle v\rangle}\equiv\frac{\sqrt{N_{avg}}}{4}\delta_v \tag{9}$$

In Equation (9), v_i is the average velocity of the ith analyte zone through the separation field, defined as $v_i=L/t_i$. As each analyte migrates through the same conduit (tube, column, etc.) with length L, $|\Delta t|/\langle t\rangle$ equals δ_v. Although in stand-alone DTIMS, zone electrophoresis or column chromatography under isocratic conditions the analytes

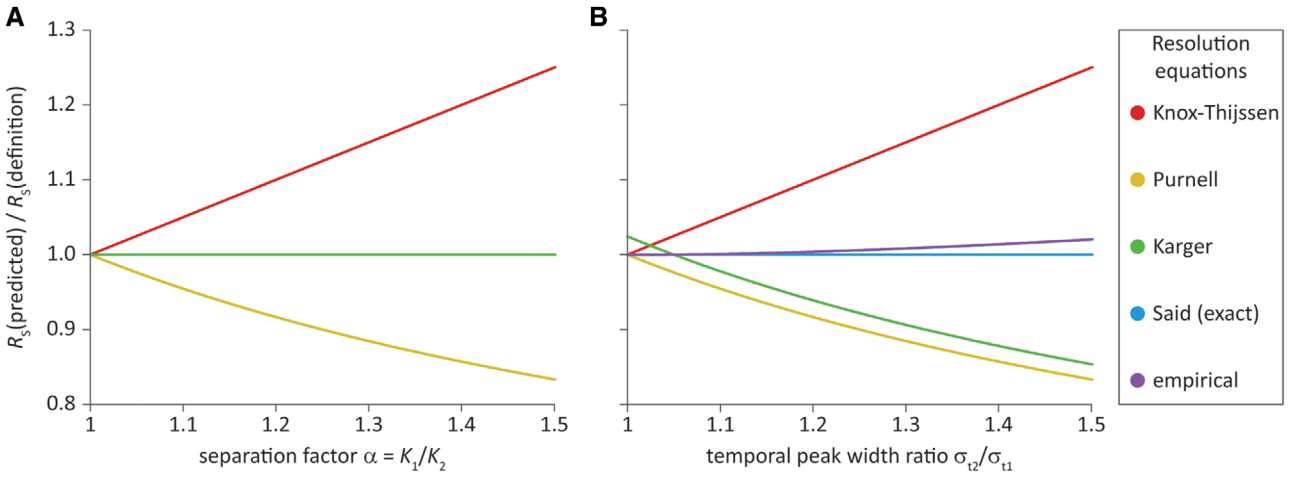

FIGURE 1 Comparison of chromatography-influenced resolution equations for drift tube ion mobility spectrometry. Peak-to-peak resolution R_S calculated according to the various predictive resolution equations for DTIMS. Equations are color coded, and the names refer to the respective chromatographic equations they derive from; in the empirical formula (purple trace), N_{avg} is approximated by the geometric mean of N_1 and N_2 (see Table 1). Calculated R_S values are divided by the exact value of R_S as defined in Equation (1), that is, a value of 1 represents perfect agreement. As $\alpha = 0$ leads to zero R_S, the plotted functions are not defined at this point. (A) Trueness of predicted R_S as a function of α, the ratio of ion mobilities. In these calculations, equal plate counts were assumed for the two components ($N_1 = N_2$); owing to the normalization of R_S values the absolute number of plates is indifferent. The exact and empirical equations would coincide with the green trace. (B) Trueness of predicted R_S as a function of the temporal peak width ratio $\sigma_{t,2}/\sigma_{t,1}$. The ratio of plate numbers changed according to the peak width ratio ($N^{1/2} \sim 1/\sigma_t$). In the calculations, α was fixed at 1.05, corresponding to 5% difference in mobilities. For calculating the green trace (equal plate number assumption), N_2 was used when the two plate counts differed

migrate at constant velocity, there is no need to assume constant velocity to arrive at the above formula. In DTIMS, δ_v is the ratio of the difference and the arithmetic mean of two drift velocities, and as such, adopts values in the range $0 \leq \delta_v < 2$. Although cases with one of the analyte zones being stagnant or the velocity vectors pointing to opposite directions are interesting on their own merit, due to their irrelevance to standard DTIMS these are not considered here in relation to δ_v. In Equations (5) and (7), δ_v is expressed using retention factors and the separation factor, α being inherited by the corresponding equations for DTIMS. Instead of relying on chromatographic parameters stemming from an analogy-driven approach, this section aims to utilize first principles and relate δ_v to fundamental parameters of IMS itself. We may look at δ_v as the operational selectivity describing the relative behavior of two analytes in a separation.

In DTIMS, the drift velocity v_d of ions is directly proportional to their mobility K, the proportionality factor being the drift field E_D. Thus, from Equation (9) applicable to various differential migration processes, we arrive at the following expression for DTIMS:

$$R_{S,DT} = \frac{\sqrt{N_{avg}}}{4} \frac{|\Delta K|}{\langle K \rangle} \tag{10}$$

This formula is very similar to its well-known counterpart for zone electrophoresis, the main differences being the appearance of gas-phase ion mobilities instead of their condensed-phase analogues, and the absence of an equivalent for the electroosmotic flow [24,25]. By employing the relation $\alpha = K_1/K_2$ [15], Equations (8) and (10) can be shown to be equivalent, providing a mutual validation. Equation (10) is exact as no assumption about peak width or plate numbers was required for the derivation, and clearly shows how R_S can be improved in practice. Besides the possibility of increasing the number of theoretical plates, which concerns instrument development to a great degree, one may try to influence the relative mobilities of the two analytes through altering the separation conditions.

To explore the latter option in more detail, let us utilize the fundamental low-field ion mobility equation and relate K to quantities more closely associated with the ion structure and characteristics of the collision complex [6,7,26,27]:

$$K = \left(\frac{18\pi}{\mu k_B T}\right)^{1/2} \frac{ze}{16N\Omega} = C\,\frac{z}{\Omega\sqrt{\mu}} \tag{11}$$

In Equation (11), μ is the reduced mass of the ion–neutral collision complex, k_B is the Boltzmann constant, T is the temperature of the buffer gas (within the low-field limit ions are assumed to be in thermal equilibrium with the gas), z is the ionic charge state, e is the elementary charge, N is the buffer gas number density, and Ω is the rotationally averaged collision integral (herein collision cross-section),

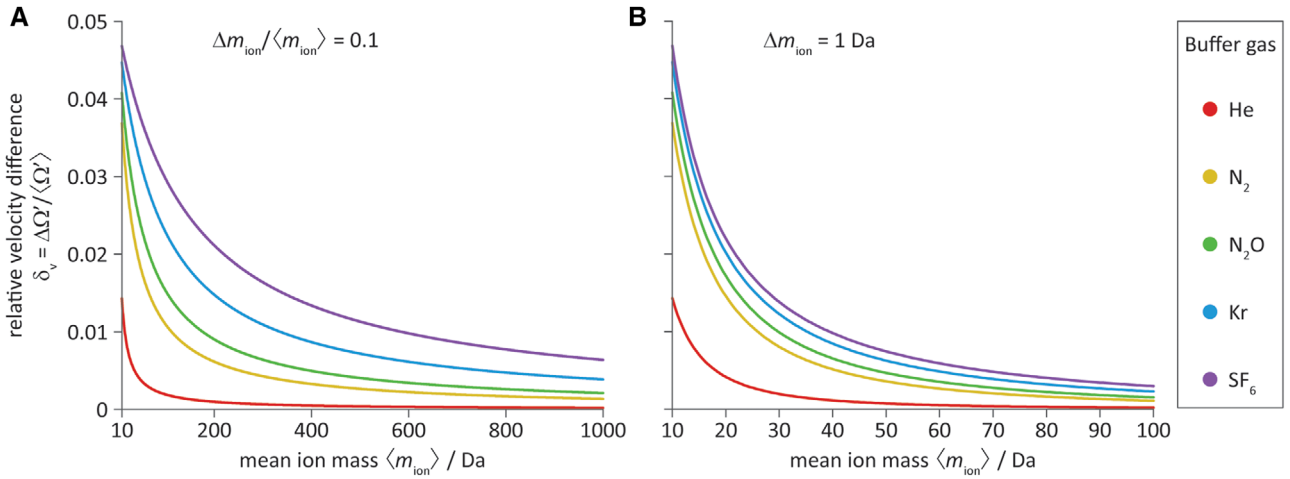

FIGURE 2 The influence of reduced mass difference on selectivity in drift tube ion mobility separations. (A) Relative velocity difference δ_v of ion pairs with identical collision cross-sections and nonidentical masses (mimicking isotopologue separations), plotted as a function of the mean ion mass. Colors encode representative buffer gases, ranging from the lightest (He) to the heaviest (SF_6) gas applied in practice. The relative mass difference of the ion pairs $\Delta m_{ion}/\langle m_{ion}\rangle$ was held constant at 0.1. (B) Analogous δ_v versus $\langle m_{ion}\rangle$ plot showing the effect of a constant absolute mass difference. Instead of keeping the relative mass difference fixed as on the left, the absolute mass difference of the ions was held at 1 Da, resulting in a more rapid drop of δ_v with increasing ion mass. Note the difference between the ion mass ranges on the two plots. For brief overview, the buffer gases used in the calculations with their rounded standard atomic/molecular weight in Da: He 4; N_2 28; N_2O 44; Kr 84; SF_6 146. In the calculations, all stable isotopes/isotopologues of the buffer gas atoms/molecules were considered, weighted with their relative abundances

an effective area related to the target size for the ion–neutral pair and the efficiency of momentum transfer upon collision [28]. Ω values reflect the ions' size and shape and are independent of instrument geometry or measurement conditions within the low-field limit, serving as comparable molecular descriptors [29,30]. Dimensionless factors, physical constants, and experimental parameters that are the same for all species can be expressed by a single integrated constant C, highlighting the dependence of K on three analyte-related quantities: z, μ, and Ω. These can be combined to yield the charge- and reduced mass-normalized collision cross-section Ω', defined as [31]:

$$\Omega' = \frac{\Omega\sqrt{\mu}}{|z|} \tag{12}$$

Ultimately, DTIMS separates gas-phase ions according to their Ω' values. Thus, employing Ω' (defined here as a positive quantity) we may reformulate Equation (10) to obtain the following expression for DTIMS:

$$R_{S,DT} = \frac{\sqrt{N_{avg}}}{4}\frac{|\Delta\Omega'|}{\langle\Omega'\rangle} \tag{13}$$

The above solution is exact and relates δ_v to the Ω' values of the analytes in the given buffer gas, which are characteristic to the ion–neutral complex and can potentially be stored in databases. Thus, Equation (13) is accurate and practical, has a high predictive potential, and reveals how δ_v can be influenced in DTIM separations, addressed in detail in the following subsections.

2.2.1 | The influence of the reduced mass on selectivity

The dependence of Ω' on μ enables analysts to optimize conditions for separations concerning ions with nonidentical masses, such as the separation of isotopes or isotopologues in stand-alone IMS. The larger the mass of the gas particles compared to the masses of the two ions, the larger the relative difference between the μ values of the respective collision complexes will be (provided the ion masses differ). Thus, δ_v may be tailored and R_S consequently improved by the adjustment of the buffer gas atomic/molecular weight for the separation of lighter ions with different masses [32,33].

Figure 2 explores in detail how differences in μ can be exploited to influence selectivity in DTIMS. To study the effect of reduced mass difference on δ_v independently of other influencing factors, Ω and z were assumed to be identical, the absolute values being irrelevant. Although kinetic theory [34,35] and some experiments [33] suggest that isotopologues may have extremely small differences in their Ω values, for practical purposes the assumption of identical Ω remains generally valid [36,37]. The two plots in

Figure 2 depict δ_v for analyte pairs with nonidentical masses as a function of their mean mass $\langle m_{ion} \rangle$. The colors represent various buffer gases, ranging from the lightest (He) to the heaviest (SF_6) gas applied in practice. It is apparent that δ_v decreases rapidly with increasing $\langle m_{ion} \rangle$, and that heavier gases lead to improved selectivity. The heavier the gas relative to the ions, the larger δ_v will be for isotopologues. In Figure 2a, the relative mass difference of ions $\Delta m_{ion}/\langle m_{ion} \rangle$ was kept constant at 0.1. For an ion pair with 10 Da average mass, it means 1 Da absolute difference, that is, 9.5 and 10.5 Da for the two species; for a pair with 100 Da mean mass, the difference is 10 Da. With the gas particles becoming heavier, the reduced mass of each collision complex approaches the mass of the respective ion. Consequently, for any given value of $\langle m_{ion} \rangle$, δ_v converges to $\Delta({m_{ion}}^{1/2})/\langle {m_{ion}}^{1/2} \rangle$ (corresponding uniformly to roughly 0.05 in Figure 2a) as the mass of the gas particles increases. It is apparent that for heavy ions the aforementioned convergence of δ_v is very slow, and the values remain low under experimentally feasible conditions ($m_{gas} < 150$ Da). In Figure 2b, the absolute mass difference between the members of each ion pair was fixed at 1 Da. Thus, $\Delta m_{ion}/\langle m_{ion} \rangle$ decreases with increasing mean ion mass, and δ_v drops even more rapidly as the analytes become heavier. Note the difference between the range of $\langle m_{ion} \rangle$ values chosen in the two plots. The above analysis did not involve gas mixtures, but the presence of multiple gas isotopes/isotopologues were considered [36,38]. Despite the simplicity of the model, the main trends and strategies to exploit differences in ion mass to improve δ_v could be revealed.

2.2.2 | The influence of the collision cross-section and the ionic charge state on selectivity

As the ratio of the Ω values for two ions may also depend on the buffer gas composition, the effect of different buffer gases [39–41] and gas-phase modifiers [42,43] on selectivity have been extensively studied. Altering the ratio of Ω values through changing or doping the buffer gas potentially enables the analyst to tailor selectivity in (low-field) IM separations, with particular relevance to isomer separations. However, in comparison to more flexible chromatographic and condensed-phase electrophoretic separations where selectivity can be influenced by tuning a myriad of parameters and conditions over a broad range, the possibilities in IMS are more restricted, and the resulting effects are less striking. It should also be mentioned that the choice of buffer gas can affect the plate count as well by influencing the absolute value of transport properties [1,2,44], which is important as R_S depends on both N_{avg} and δ_v.

Arguably the most important application of IMS and IM-MS is the separation of isomers, where differences in Ω represent the only aspect of selectivity. As μ is the same for isomeric species, Equation (13) can be simplified (assuming the two analytes have the same charge):

$$R_{S,DT} = \frac{\sqrt{N_{avg}}}{4} \frac{|\Delta\Omega|}{\langle\Omega\rangle} \tag{14}$$

Equation (14) is very similar to that proposed by Dodds et al. [45], the only difference being the appearance of N_{avg}, the effective average plate number defined according to Equation (6). Equations (13) and (14) can also be utilized to calculate the number of theoretical plates required to achieve certain R_S for a given analyte pair, as shown in Figure 3. The plots highlight the intertwined influence of resolving power (expressed by N_{avg}) and selectivity (expressed by $\Delta\Omega'/\langle\Omega'\rangle$) on the ultimately achieved peak resolution in DTIMS. In general, $R_S = 0.75$ is required to readily distinguish two peaks, whereas $R_S = 1.5$ marks baseline separation by convention. As cutting-edge high-pressure DTIMS instruments may achieve plate numbers on the order of 10^5 [2], separating isomers with roughly 0.5–1% collision cross-section difference represents the current limit of this technique.

High kinetic energy (HiKE) IMS [46], FAIMS [47], or its recent variation, field asymmetric time-of-flight (FAT) IMS [48], exploit energetic hyperthermal collisions in high fields and the resulting dependence of K and Ω on the reduced field strength to influence selectivity. Although this approach is effective and orthogonal to that of changing the buffer gas, it transcends the boundaries of linear low-field IMS and therefore not discussed further.

There is little playing field for the analyst to influence z selectively, but its effect is important to understand and predict R_S for ions having the same m/z but different mass and charge, such as various oligomers. In the discussion above, the separation of isotopologues, isomers and oligomers serve as representative examples. In most analytical problems, especially those concerning stand-alone IMS, it is the combined effect of μ, Ω, and z that needs to be evaluated in relation to selectivity, as expressed by the single parameter Ω' in Equation (13).

As a final remark to Section 2.2, in relation to Equations (10), (13), and (14), we shall briefly address the possibility of predicting selectivity in DTIMS relying solely on theoretical approaches. First, state-of-the-art computational methods are capable of generating correct structural models for gas-phase molecular ions of ever-increasing complexity. Second, two-body interactions governing separation in IMS are much more amenable to computational treatment than many-body encounters determining retention in chromatography [49]. If the aforementioned

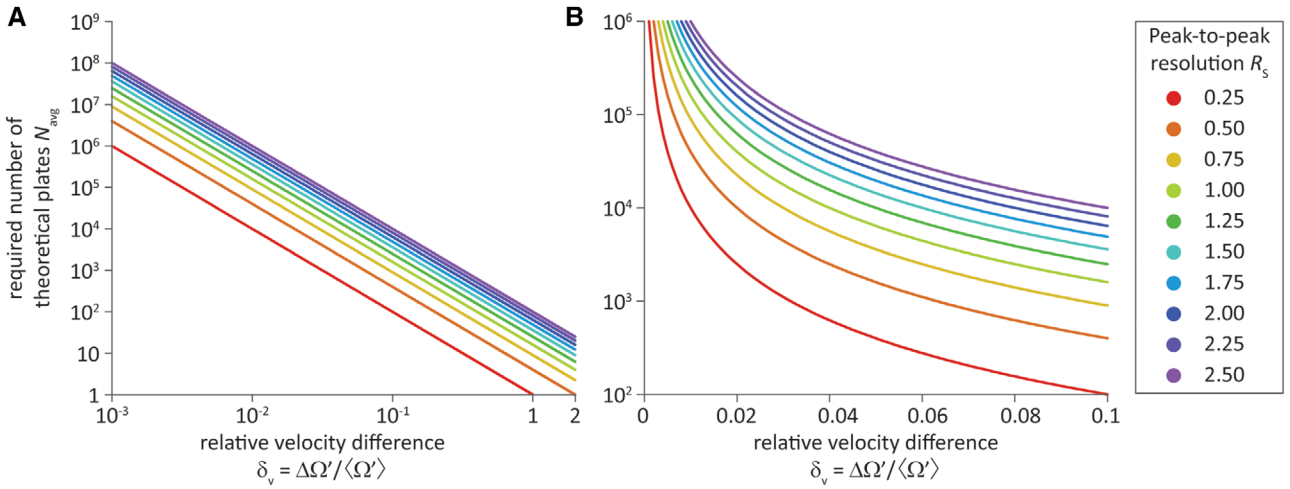

FIGURE 3 Number of theoretical plates needed for achieving defined resolution between two peaks in drift tube ion mobility spectrometry. (A) Double-log plot showing the effective average number of plates N_{avg} required to reach defined R_S values as a function of the analytes' relative velocity difference δ_v. It is worth mentioning that δ_v adopts nonnegative values below 2 in drift tube ion mobility separations, but values close to this theoretical upper limit are of little practical relevance. $R_S = 1.5$ corresponds to baseline separation; an n-fold increase in R_S requires an n^2-fold increase in N_{avg}. (B) Single-log plot highlighting the most relevant and experimentally accessible region. Most separations in practice concern analyte pairs with $\delta_v < 0.1$. At present, state-of-the-art high-pressure linear DTIMS instruments may achieve theoretical plates on the order of 10^5

suitable ion structures are available, Ω and K can be calculated in a variety of buffer gases with satisfying accuracy [50–55]. Thus, with increasing computational power and further progress of theoretical methods, the prospect of predicting selectivity in DTIMS entirely computationally, at least for simpler systems, does not seem far fetched.

2.3 | From stand-alone ion mobility spectrometry to ion mobility-mass spectrometry

In our analysis so far, we implicitly assumed that ion drift related post-cell effects—the analogues of extra-column factors in chromatography—are absent. This may be true for stand-alone IMS (although detector rise time is still important), but is not entirely valid in IM-MS where ions may traverse ion funnels, ion guides, and mass analyzers before reaching the detector. The residence time of ions in these post-cell compartments adds to their net drift time t_D, the sum being the total arrival time t_A. As mobility-based separation does not take place in many of these post-cell compartments, their presence affects the calculation of R_S.

Post-cell effects on R_S can be incorporated into the expression of plate numbers, as shown below. Let us adopt the dimensionless factor F from [1] as the fraction of non-separative transport time t_{NS} in relation to the total arrival time t_A:

$$F = \frac{t_{NS}}{t_A} = \frac{t_{NS}}{t_S + t_{NS}} \tag{15}$$

In Equation (15), t_A was divided into a separative part t_S during which ions are separated according to their mobilities, and into a nonseparative part t_{NS} with no separation taking place, that is, t_{NS} is assumed to be the same for any two neighboring species. In general, residence time of ions in the mobility cell and the exit funnel (if present) amount to t_S, while t_{NS} comprises the residence times in post-cell compartments under high vacuum. Such explicit categorization of compartments is physically justified. First, pressure and temperature across a mobility cell and the corresponding exit funnel are uniform because no conductance limit is present between them. It means that ion mobilities are left unchanged and δ_v is the same in these compartments, even if the absolute velocities may differ (low-field conditions are assumed). Second, additional separation of two neighboring ion clouds in ion guides, etc., following the drift region is not very significant, especially if the ions have identical or similar m/z ratios. Therefore, employing $\Delta t_{NS} = 0$ for these compartments introduces a negligible error in the calculations. Using F, we can define the apparent plate number for DTIM-MS:

$$N_{app} = \left(\frac{t_A}{\sigma_t}\right)^2 (1-F)^2 = \left(\frac{t_S}{\sigma_t}\right)^2 \tag{16}$$

The numerator of N_{app} correctly accounts for those compartments only where mobility separation takes place.

Because in compartments not contributing to separation Δt_{NS} is zero in our assumption, Δt_A appears equal to Δt_S. Thus, by substituting t_A instead of t_D into Equation (1), the general expression for R_S in the presence of post-cell compartments can be obtained:

$$R_S = \frac{\Delta t_A}{4\langle\sigma_t\rangle} = \frac{\langle t_S\rangle}{4\langle\sigma_t\rangle}\frac{\Delta t_S}{\langle t_S\rangle} = \frac{\sqrt{N_{app}}}{4}\delta_v \tag{17}$$

Here, N_{app} is the effective average plate number corrected with F according to Equation (16). Since δ_v in the mobility cell and the respective exit funnel is the same, the DTIM-MS specific predictive equation for R_S appears as:

$$R_{S,DT} = \frac{\sqrt{N_{app}}}{4}\frac{|\Delta\Omega'|}{\langle\Omega'\rangle} \tag{18}$$

2.4 | Peak-to-peak resolution in traveling wave ion mobility separations

In this section, we aim to find a predictive resolution equation for TWIMS [56,57] by extending the approach employed for DTIMS before. The main difference between the two techniques concerns selectivity and δ_v. Although in DTIMS drift velocities are directly proportional to K, in TWIMS this dependence is nonlinear and cannot be traced back to first principles [58]. Hence, Equation (10) and subsequent formulae derived from it are not applicable to the latter method.

A widely applied solution to the above problem is to transfer TWIM separations from their fundamental temporal dimension into the collision cross-section domain, that is, accounting for the altered selectivity by including its effect into a modified Ω-based definition of N or R_P [45]. This approach has several advantages, but ultimately blurs the clear distinction between two independent aspects of peak resolution: plate count/resolving power and δ_v. The method-specific, rather arbitrary modification of fundamental definitions (N and R_P) also leads to some dissonance between this approach and the unified theoretical toolbox of separation methods [8].

Here, we provide a solution that is mathematically equivalent to the one mentioned above, but adheres to the general formalism of separation science. To obtain the desired formula for TWIMS, a suitable expression for δ_v needs to be found and substituted into Equation (9). In general, the following power function is employed for collision cross-section calibration in TWIMS, that is, to describe the dependence between Ω' and the ion transit time (post-cell effects being neglected) [31,59]:

$$\Omega' = A(t_D)^B \tag{19}$$

In Equation (19), t_D is the transit time of ions through the TWIMS cell, while A and B are parameters that depend on experimental conditions. A and B are determined experimentally during the general collision cross-section calibration process using suitable calibrants [60,61]. Employing this semiempirical relation to express δ_v and the notation $1/B = \gamma$, the predictive resolution equation for TWIMS appears as:

$$R_{S,TW} = \frac{\sqrt{N_{avg}}}{4}\frac{\left({\Omega'_2}^{\gamma} - {\Omega'_1}^{\gamma}\right)}{\langle\Omega'^{\gamma}\rangle} \tag{20}$$

The subscript in $R_{S,TW}$ indicates the TWIMS specificity of Equation (20). The exponent γ accounts for the altered selectivity in TWIM separations. In DTIMS γ equals 1, while in TWIMS it generally exceeds unity in practice, with clearly favorable consequences to δ_v and R_S. Besides determination through calibration, this factor may be estimated theoretically for close-lying peaks under certain assumptions. As an illustrative example, for symmetric triangular waveforms γ adopts a value of 2 if the maximum ion velocity is much lower than the wave velocity [58,62].

As of today, no complete analytical description of ion motion in TWIMS cells operated with discretely stepping potential waves is available, making the technique dependent on suitable calibrants for most applications. However, a detailed model for hypothetical smoothly moving waves has been developed [62], marking a significant step toward the ultimate goal of TWIMS theory: an exact equation derived from first principles, describing the universal relation between K and the ion velocity. Once such description is available, it will be possible to place selectivity on entirely theoretical foundations in TWIM separations.

2.5 | Peak capacity in ion mobility separations

Having addressed peak-to-peak resolution, we may build on these findings and explore peak capacity (P_C) in IM separations. P_C was conceived originally by Giddings for elution chromatography [63], but may be readily transferable to other differential migration methods owing to the abstract mathematical nature of the concept. P_C represents the maximum number of resolved peaks that can be fit into the separation window, for example, chromatogram, electropherogram, or ion mobility spectrum. It reflects the hypothetical case when peaks are ideally distributed,

meaning that R_S is the same for any two neighboring peaks within a single dimension of the separation window. Although the exact value of R_S may be chosen arbitrarily, in general it is defined to be 1 or 1.5 for practical reasons: values lower than unity would express significant peak overlap, whereas values higher than that of baseline separation would correspond to the suboptimal utilization of the time window with unoccupied spaces between peaks. In addition to the predefined value of R_S, P_C depends on two factors: The width of the peaks and the actively utilized size of the separation window. The narrower the peaks and the larger this window, the higher the peak capacity. Due to nonideal, often random distribution of peaks in real separations, the number of resolved components in reality is merely a fraction of this number as shown by Poisson statistics [64,65]. Thus, P_C may be viewed as an estimate of the total number of resolvable components, serving as a comprehensive measure of the overall separation performance. P_C is arguably the most suitable index to compare separation methods: electrophoretic techniques may generate extremely high plate counts, but the separation window in these methods is rather narrow in comparison to chromatography, both in the liquid and the gas phase. For this reason, it is essential to obtain a suitable model for peak capacity in IMS.

As mentioned above, the maximum number of resolved peaks n in the separation window depends on the peaks' temporal width (σ_t), the desired resolution between them ($R_{S,fix}$, the subscript referring to the fixed, predefined nature of this parameter), as well as on the breadth of the window spanning from the first to the nth peak [66]:

$$\frac{dn}{dt_D} = \frac{1}{4R_{S,fix}\sigma_t(t_D)} \tag{21}$$

$$\int_1^n dn = \frac{1}{4R_{S,fix}} \int_{t_{D,1}}^{t_{D,n}} \frac{dt_D}{\sigma_t(t_D)} \tag{22}$$

Here, $\sigma_t(t_D)$ emphasizes the potential variation of the peak width across the separation window as a function of the drift time. From Equation (22), one can obtain the mathematical definition of peak capacity in its general integral form [67]:

$$P_{C,def} = n = 1 + \frac{1}{4R_{S,fix}} \int_{t_{D,1}}^{t_{D,n}} \frac{dt_D}{\sigma_t(t_D)} \tag{23}$$

To highlight the dependence of P_C on the plate count, Equation (23) can be rewritten using $N = (t_D/\sigma_t)^2$, where N may also be a function of t_D:

$$P_{C,def} = 1 + \frac{1}{4R_{S,fix}} \int_{t_{D,1}}^{t_{D,n}} \frac{\sqrt{N(t_D)}}{t_D} dt \tag{24}$$

The way N and σ_t depend on t_D is central to the peak capacity problem. Solving Equation (23) or (24) to yield the desired expression for P_C requires the explicit form of $N(t_D)$ or $\sigma_t(t_D)$ be known. In the following sections, two approximate solutions based on well-known assumptions borrowed from chromatography, as well as an exact solution derived from a suitable physical model for peak broadening in DTIMS, will be presented.

2.5.1 | The constant plate number assumption

Assuming that N is the same for each analyte and independent of t_D, that is, $\sigma_t(t_D) = t_D(N)^{1/2}$ where N is constant, the solution of Equation (24) is straightforward and yields the following expression:

$$P_{C,N} = 1 + \frac{\sqrt{N}}{4R_{S,fix}} \int_{t_{D,1}}^{t_{D,n}} \frac{1}{t_D} d\, t_D = 1 + \frac{\sqrt{N}}{4R_{S,fix}} \ln\frac{t_{D,n}}{t_{D,1}} \tag{25}$$

In Equation (25), $t_{D,1}$ and $t_{D,n}$ correspond to the first and last peak, respectively, while the subscript of $P_{C,N}$ implies that N was assumed to be constant. It is worth mentioning at this point that none of the peak capacity-related equations presented so far is specific for IMS. Upon changing t_D to t_R, Equation (25) becomes identical to the simple formula for isocratic elution chromatography [63,66,67].

From the inverse proportionality between K and t_D in DTIMS, or K and t_A in DTIM-MS, a more revealing formula arises that is specific for the aforementioned technique:

$$P_{C,N,DT} = 1 + \frac{\sqrt{N}}{4R_{S,fix}} \ln\frac{K_1}{K_n} \tag{26}$$

The error stemming from ignoring the mobility-independent contributions to t_A in DTIM-MS is negligible. Ω' may also be used to express the ratio of drift and arrival times, resulting in the following practical expression for DTIMS and DTIM-MS:

$$P_{C,N,DT} = 1 + \frac{\sqrt{N}}{4R_{S,fix}} \ln\frac{\Omega'_n}{\Omega'_1} \tag{27}$$

For separations utilizing the traveling wave technique, Equation (27) can be modified according to Equation (19) and employing the notation $1/B = \gamma$:

$$P_{C,N,TW} = 1 + \frac{\sqrt{N}}{4R_{S,fix}} \gamma \ln \frac{\Omega'_n}{\Omega'_1} \tag{28}$$

Equation (28) makes it apparent that for the same ratio of Ω' values and same N—defined based on the temporal or spatial SD of peaks, not on their width in a Ω-space—$P_{C,N}$ will be higher for TWIMS than for DTIMS by the factor γ (neglecting the constant 1 on the right-hand side). Practical values of γ normally fall in the range between 1.5 and 2 [60,61]. Owing to the nonlinear dependence of t_D on Ω', the time window in a TWIM separation will be broader in relation to the σ_t of peaks than in an analogous DTIM separation. Consequently, the TWIM spectrum will be capable of encompassing more resolved components provided N is the same.

2.5.2 | The constant temporal peak width assumption

Let σ_t be constant across the whole separation window, meaning that $N(t_D) = (t_D/\sigma_t)^2$ where σ_t is independent of the drift time. In this case, the solution of Equation (23) appears as:

$$P_{C,\sigma} = 1 + \frac{1}{4R_{S,fix}\sigma_t} \int_{t_{D,1}}^{t_{D,n}} dt_D = 1 + \frac{1}{4R_{S,fix}\sigma_t} (t_{D,n} - t_{D,1}) \tag{29}$$

The subscript denotes σ_t being a constant. Alternatively, employing $\sigma_t = t_{D,1}/(N_1)^{1/2}$ where N_1 is the plate count for the first peak, Equation (29) can be rewritten as:

$$P_{C,\sigma} = 1 + \frac{\sqrt{N_1}}{4R_{S,fix}} \left(\frac{t_{D,n} - t_{D,1}}{t_{D,1}} \right) \tag{30}$$

Equations (29) and (30) are analogous to the simple expressions derived for gradient elution chromatography [66–68]. From the general expression above we can obtain equations specific for DTIM separations:

$$P_{C,\sigma,DT} = 1 + \frac{\sqrt{N_1}}{4R_{S,fix}} \left(\frac{K_1 - K_n}{K_n} \right) \tag{31}$$

$$P_{C,\sigma,DT} = 1 + \frac{\sqrt{N_1}}{4R_{S,fix}} \left(\frac{\Omega'_n - \Omega'_1}{\Omega'_1} \right) \tag{32}$$

For TWIM separations the respective equation appears as:

$$P_{C,\sigma,TW} = 1 + \frac{\sqrt{N_1}}{4R_{S,fix}} \left(\frac{{\Omega'_n}^{\gamma} - {\Omega'_1}^{\gamma}}{{\Omega'_1}^{\gamma}} \right) \tag{33}$$

Thus, γ values exceeding unity will lead to an increase in $P_{C,\sigma}$.

2.5.3 | An exact peak capacity equation for drift tube ion mobility spectrometry based on the injection-diffusion model of zone broadening

Although equations based on the constant N and the constant σ_t assumptions are certainly helpful, their value lies mostly in their simplicity. In DTIM separations, assuming N being the same for all species may be justified if diffusion is the dominant dispersion process and the initial spread of the injected ion cloud is negligible. On the other hand, the constant peak width assumption may be valid if σ_t is determined predominantly by the injection pulsewidth, with subsequent diffusional broadening being negligible. In practice, however, the contributions of these two sources are generally comparable, especially under conditions where resolving power is expected to be highest [1,69]. As such, the above P_C equations have limited applicability in the experimentally most relevant cases.

To overcome these limitations and derive an exact, universally applicable P_C equation for DTIM separations, a suitable physical model of zone dispersion needs to be considered. The two major sources of peak broadening in DTIM separations are diffusion and the finite width of the injected ion packets. Being independent processes, the associated variances are additive yielding [1]:

$$\sigma_{t,ID}(t_D) = \left(\sigma^2_{t,inj} + \sigma^2_{t,diff}(t_D) \right)^{1/2} = \left(\sigma^2_{t,inj} + t_D^2 \frac{2k_B T}{|z|eV_D} \right)^{1/2} = \left(\sigma^2_{t,inj} + \frac{t_D^2}{N_{diff}} \right)^{1/2} \tag{34}$$

The above variance components are analogous to those in zone electrophoresis assuming linear conditions [23,25,70]. From Equation (34), the corresponding total plate count N_{ID} can be readily calculated as:

$$N_{ID}(t_D) = \frac{t_D^2}{\sigma^2_{t,inj} + \frac{t_D^2}{N_{diff}}} \tag{35}$$

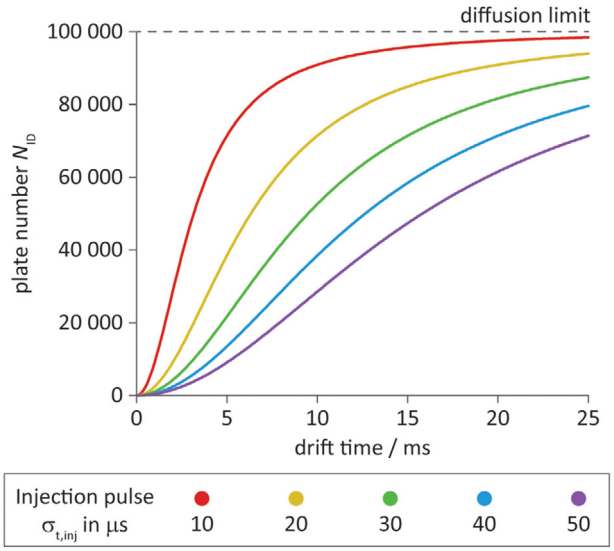

FIGURE 4 Systematic variation in the number of theoretical plates across a single drift tube ion mobility spectrum. Considering the finite width of the injection pulse and subsequent diffusional broadening of the ion packets, the plate count N_{ID} will appear different for each peak within a single separation at fixed drift voltage. The plate number achieved for a given analyte will depend on its drift time, which is inversely proportional to the ion's mobility. The calculations rely on the assumption that all ions have the same charge state. The diffusion limit of theoretical plates was set at 100 000 (black dashed line), corresponding to roughly 5.14 kV drift voltage for singly charged ions at room temperature. Each color-coded curve represents a different value of $\sigma_{t,inj}$, the temporal standard deviation associated with the injection pulse. At extremely short drift times the functions bear little practical relevance and should be interpreted carefully: For ions with very high mobilities the reduced field will inevitably exceed the low-field limit

In the above equations, $\sigma_{t,ID}$ is the total temporal SD of a given peak, the subscript referring to the injection-diffusion physical model. Temporal variances $(\sigma_{t,inj})^2$ and $(\sigma_{t,diff})^2$ express the contribution of injection and diffusion, respectively. The dependence of $\sigma_{t,diff}$, $\sigma_{t,ID}$ and N_{ID} on t_D is shown explicitly, k_B being the Boltzmann constant, T the temperature of the buffer gas and ions, $|z|$ the absolute value of the ionic charge state, e the elementary charge and V_D the drift voltage. Employing N_{diff}, the diffusion limit of theoretical plates, a more concise expression ensues. As z is the only analyte-specific quantity influencing N_{diff}, Equations (34) and (35) adequately describe peak broadening and the plate count for a set of ions having the same charge state. Owing to their relatively small contribution to peak broadening, space charge effects were not included into Equations (34) and (35). Figure 4 highlights the variation of N_{ID} across the separation window as a function of t_D. In other words, it reflects the dependence of the plate count on the ions' mobility in a single DTIM spectrum with V_D and N_{diff} held constant.

Upon substituting Equation (34) into Equation (23), or Equation (35) into Equation (24), we obtain:

$$P_{C,ID,DT} = 1 + \frac{1}{4R_{S,fix}} \int_{t_{D,1}}^{t_{D,n}} \frac{dt_D}{\left(\sigma_{t,inj}^2 + \frac{t_D^2}{N_{diff}}\right)^{1/2}} \tag{36}$$

In Equation (36), the subscript of $P_{C,ID,DT}$ refers again to the underlying physical model and the resulting DTIMS specificity of the formula. The solution of Equation (36) can be traced back to the following basic integral [71]:

$$\int \frac{1}{\sqrt{1+x^2}}\, dx = \operatorname{arsinh}(x) = \ln\left(x + \sqrt{x^2+1}\right) \tag{37}$$

Here, arsinh is the inverse or area hyperbolic sine function (the constant of integration was omitted). Thus, the solution of Equation (36) takes the following form (step-by-step derivation can be found in the Supporting Information, Section S3):

$$P_{C,ID,DT} = 1 + \frac{\sqrt{N_{diff}}}{4R_{S,fix}} \ln \frac{t_{D,n} + \left(t_{D,n}^2 + N_{diff}\sigma_{t,inj}^2\right)^{1/2}}{t_{D,1} + \left(t_{D,1}^2 + N_{diff}\sigma_{t,inj}^2\right)^{1/2}} \tag{38}$$

An important aspect of N_{diff} is that it adopts the same value for all species within a given charge state. It is worth mentioning that—owing to similarities in the underlying mathematics—Equation (38) resembles the peak capacity equation in chromatography when extra-column band broadening is considered [72].

As a verification of Equation (38), the exact peak capacity equation for DTIMS, let us examine its behavior at limiting cases. If $\sigma_{t,inj}$ is assumed to be zero (infinitesimally short injection), Equation (38) becomes:

$$P_{C,D,DT} = 1 + \frac{\sqrt{N_{diff}}}{4R_{S,fix}} \ln \frac{t_{D,n}}{t_{D,1}} \tag{39}$$

The subscript of $P_{C,D,DT}$ indicates that only diffusion was considered, the initial width of the ion packet being neglected. Equation (39) is analogous to Equation (25), obtained by assuming constant N on the basis that diffusion is the dominant dispersion process.

At the other extreme, $\sigma_{t,diff}$ is negligibly small compared to $\sigma_{t,inj}$. In this case, employing the Maclaurin series of arsinh(x), Equation (38) can be simplified to the following

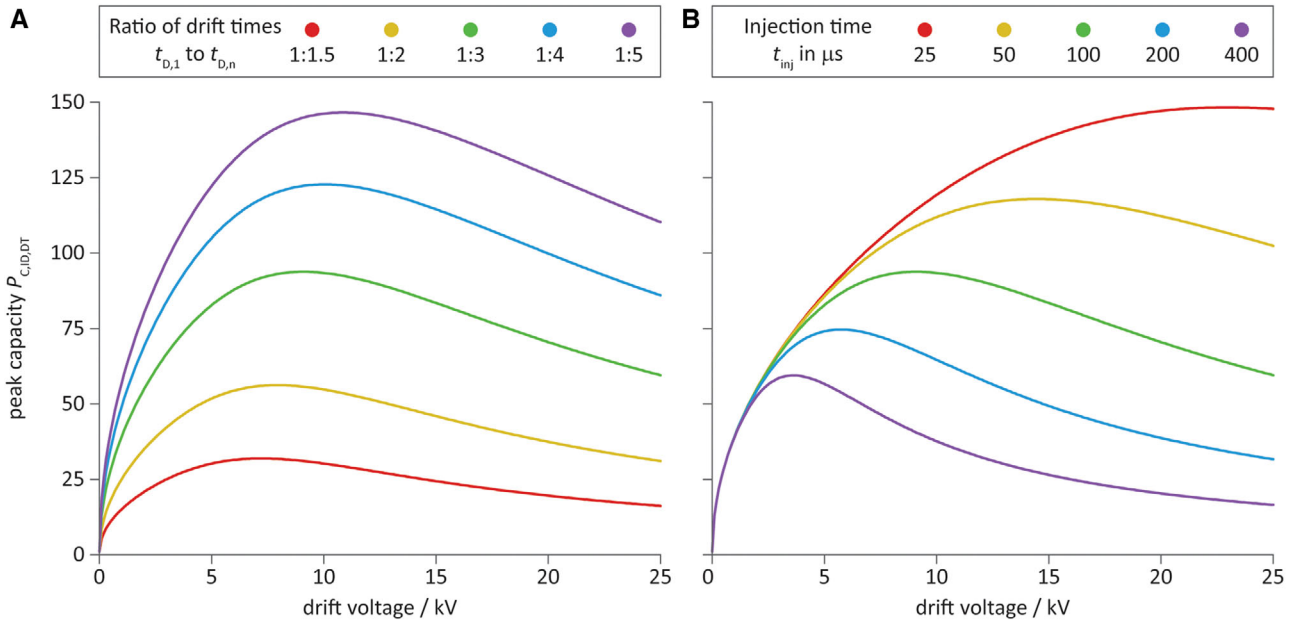

FIGURE 5 Peak capacity in drift tube ion mobility spectrometry based on the injection-diffusion model. Peak capacity $P_{C,ID,DT}$ calculated according to the exact formula Equation (38) and depicted as a function of drift voltage V_D. (A) Curves are color-coded according to the drift time ratio between the first and the last peak; t_{inj} was fixed at 100 µs. (B) Colors encode different injection times t_{inj}, varied from 25 to 400 µs forming an equirational progression, and the drift time ratio was chosen to be 1:3. The two green curves are therefore identical. Calculations on both panels mimic real-life drift tube ion mobility separations, performed at 293.15 K in a 150 mm long drift cell using N_2 or air as buffer gas at atmospheric pressure. Ions were assumed to be singly charged, and $R_{S,fix}$ was chosen to be unity. Ion mobility of the first species was fixed at 2.5×10^{-4} m^2 $V^{-1}s^{-1}$, the mobility of the last species was changed according to the defined drift time ratio

form:

$$P_{C,I,DT} = 1 + \frac{1}{4R_{S,fix}\sigma_{t,inj}}\left(t_{D,n} - t_{D,1}\right)$$

$$= 1 + \frac{\sqrt{N_{inj,1}}}{4R_{S,fix}}\left(\frac{t_{D,n} - t_{D,1}}{t_{D,1}}\right) \quad (40)$$

Details of the series expansion can be found in the Supporting Information, Section S3. The subscript of $P_{C,I,DT}$ reflects the elimination of diffusion from the model, leaving injection the only source of dispersion considered. $N_{inj,1}$ is the plate count for the first peak and equals $(t_{D,1}/\sigma_{t,inj})^2$. Equation (40) appears equivalent to Equation (30), which was obtained by assuming constant temporal peak width determined by a t_D-independent dispersion process, i.e. the duration of the injection pulse.

Figure 5 explores peak capacity in DTIMS based on the injection-diffusion model and Equation (38), highlighting the influence of the most important experimental parameters, such as the applied drift voltage V_D or the injection time t_{inj}. The latter is the actual experimentally controlled duration of the injection pulse, and the respective SD can be readily calculated using the formula $\sigma_{t,inj} = t_{inj}/\sqrt{12}$, assuming rectangular pulse profile [1,25]. As V_D influences both N_{diff} as shown in Equation (34), as well as the drift time through the relation $t_D = L_D{}^2/(KV_D)$, the impact of V_D on $P_{C,ID,DT}$ is double-edged. Although $P_{C,ID,DT}$ depends on several factors in a complex manner shown by Equation (38), the most important trends are revealed by Figure 5. The portrayed calculations mimic real-life DTIM separations in every aspect, with K values chosen to reflect atmospheric pressure experiments. It is evident that a broader separation window may encompass more peaks (Figure 5a). In contrast to chromatography, however, the analyst has little control over this aspect of separation in DTIMS. In general, factors that efficiently increase N_{ID} across the whole spectrum also lead to higher $P_{C,ID,DT}$, such as employing shorter injection times as shown in Figure 5b. Albeit less obvious, the influence of the buffer gas pressure is highly important. Higher pressure leads to lower absolute mobilities, manifesting in longer drift times without altering $\sigma_{t,inj}$ or N_{diff}. Thus, raising the pressure ultimately results in increased N_{ID} and $P_{C,ID,DT}$ values. Similarly to resolving power or theoretical plates, $P_{C,ID,DT}$ reaches a maximum at an optimal V_D. The positions of these maxima along the abscissa fall between the V_D values where plate counts for the first and last peak are highest (data not shown).

Being the solution of Equation (36), we may view Equation (38) as a formula accounting for the variation of the plate count across the whole DTIM spectrum. When

relying merely on resolving power and plate count, experimental conditions such as V_D, t_{inj} or the buffer gas pressure are optimized considering a single, arbitrarily chosen component of the mixture. Peak capacity, on the other hand, enables one to optimize the separation considering the whole set of separands. Thus, it serves as a more comprehensive index of the separation performance, and a better guide for the analyst dealing with a large number of analytes simultaneously.

3 | CONCLUDING REMARKS

By merging appropriate mathematical concepts borrowed from chromatography with the physical principles of DTIM separations, approximate and exact equations were derived for peak-to-peak resolution and peak capacity.

In relation to peak-to-peak resolution, existing chromatography-influenced equations for DTIMS were evaluated and refined (Section 2.1). Employing resolution equations stemming from first principles, most importantly Equation (13), selectivity and relative velocity difference could be directly linked to the normalized collision cross-section of ions. Through revealing key factors influencing R_S, these predictive formulae may significantly benefit method optimization in everyday practice. Equations obtained for stand-alone linear DTIMS were also extended to DTIM-MS (Section 2.3) and TWIMS (Section 2.4). Through the factor γ, which reappears in expressions for peak capacity as well, Equation (20) successfully accounts for the altered selectivity in TWIM separations.

In Section 2.5, simple peak capacity equations were obtained for DTIM and TWIM separations based on the constant N and constant σ_t assumptions, borrowed from chromatography. As the range of applicability and validity of these approximate solutions is limited, an exact formula for peak capacity, Equation (38), was derived for DTIMS considering the injection-diffusion model of peak broadening. The peak capacity equations derived herein may prove to be especially fruitful in applications utilizing stand-alone IMS without MS analysis, and in general when dealing with extremely complex samples. In addition to making the calculation and optimization of peak capacity within a single IM separation more accurate and transparent, the equations will also benefit the estimation of overall peak capacity in multidimensional workflows incorporating DTIMS/TWIMS [65].

By further extending the plate-height model of IM-MS, the present study may also serve as a small step toward wholly integrating this emerging analytical technique into the unified language of separation science.

ACKNOWLEDGMENTS

The authors gratefully acknowledge financial support from the Freie Universität Berlin and the Max Planck Society. This research was funded by the German Research Foundation within the framework of the research unit FOR 2177 ("Integrated Chemical Micro Laboratories") project number PA 1766/3-1.

CONFLICT OF INTEREST

The authors have declared no conflict of interest.

REFERENCES

1. Grabarics M, Lettow M, Kirk AT, von Helden G, Causon TJ, Pagel K. Plate-height model of ion mobility-mass spectrometry. Analyst. 2020;145:6313–33.
2. Kirk AT, Bohnhorst A, Raddatz CR, Allers M, Zimmermann S. Ultra-high-resolution ion mobility spectrometry—Current instrumentation, limitations, and future developments. Anal Bioanal Chem. 2019;411:6229–46.
3. May JC, McLean JA. Ion mobility-mass spectrometry: Time-dispersive instrumentation. Anal Chem. 2015;87:1422–36.
4. D'Atri V, Causon T, Hernandez-Alba O, Mutabazi A, Veuthey JL, Cianferani S, Guillarme D. Adding a new separation dimension to MS and LC–MS: What is the utility of ion mobility spectrometry? J Sep Sci. 2017;41:20–67.
5. Revercomb HE, Mason EA. Theory of plasma chromatography/gaseous electrophoresis. Review Anal Chem. 1975;47:970–83.
6. Mason EA, McDaniel EW. Transport properties of ions in gases. 1st ed. New York: Wiley; 1988.
7. Viehland LA. Gaseous ion mobility, diffusion, and reaction. 1st ed. New York: Springer; 2018.
8. Giddings JC. Unified separation science. 1st ed. New York: Wiley; 1991.
9. Glueckauf E. Theory of chromatography. Part 9. The "theoretical plate" concept in column separations. Trans Faraday Soc. 1955;51:34–44.
10. Dose EV, Guiochon G. Normalized measure of overlap between non-Gaussian chromatographic peaks. Anal Chem. 1990;62:174–81.
11. Dvořák M, Svobodová J, Dubský P, Riesová M, Vigh G, Gaš B. Equivalent peak resolution: Characterization of the extent of separation for two components based on their relative peak overlap. Electrophoresis. 2015;36:646–54.
12. Purnell JH. The correlation of separating power and efficiency of gas-chromatographic columns. J Chem Soc. 1960;256:1268–74.
13. Knox JH. The speed of analysis by gas chromatography. J Chem Soc. 1961;77:433–41.
14. Thijssen HAC. Gas—liquid chromatography a contribution to the theory of separation in open hole tubes. J Chromatogr A. 1963;11:141–50.
15. Asbury GR, Hill HH. Evaluation of ultrahigh resolution ion mobility spectrometry as an analytical separation device in chromatographic terms. J Microcolumn Sep. 2000;12:172–8.
16. Rathore AS, Horváth C. Separation parameters via virtual migration distances in high-performance liquid chromatography, cap-

illary zone electrophoresis and electrokinetic chromatography. J Chromatogr A. 1996;743:231–46.
17. Karger BL. A critical examination of resolution equations for gas-liquid chromatography I. Generalized equations for linear elution conditions. J Chromatogr Sci. 1967;5:161–9.
18. Said AS. Resolution, separability, and conditions for fraction collection in preparative gas chromatography. J Chromatogr Sci. 1964;2:60–71.
19. Said AS. On the multiplicity of resolution equations in the chromatographic literature. Sep Sci Technol. 1978;13:647–79.
20. Suematsu K, Okamoto T. Problems on resolution. J Chromatogr Sci. 1989;27:13–7.
21. Giddings JC. Resolution and optimization in gel filtration and permeation chromatography. Anal Chem. 1968;40:2143–9.
22. Foley JP. Resolution equations for column chromatography. Analyst. 1991;116:1275–9.
23. Giddings JC. Generation of variance, "theoretical plates," resolution, and peak capacity in electrophoresis and sedimentation. Sep Sci Technol. 1969;4:181–9.
24. Jorgenson JW, Lukacs KD. Zone electrophoresis in open-tubular glass capillaries. Anal Chem. 1981;53:1298–302.
25. Huang X, Coleman WF, Zare RN. Analysis of factors causing peak broadening in capillary zone electrophoresis. J Chromatogr A. 1989;480:95–110.
26. Mason EA, Schamp HW. Mobility of gaseous ions in weak electric fields. Ann Phys. 1958;4:233–70.
27. Gabelica V, Shvartsburg AA, Afonso C, Barran P, Benesch JLP, Bleiholder C, Bowers MT, Bilbao A, Bush MF, Campbell JL, Campuzano IDG, Causon T, Clowers BH, Creaser CS, De Pauw E, Far J, Fernandez-Lima F, Fjeldsted JC, Giles K, Groessl M, Hogan CJ, Hann S, Kim HI, Kurulugama RT, May JC, McLean JA, Pagel K, Richardson K, Ridgeway ME, Rosu F, Sobott F, Thalassinos K, Valentine SJ, Wyttenbach T. Recommendations for reporting ion mobility mass spectrometry measurements. Mass Spectrom Rev. 2019;38:291–320.
28. Siems WF, Viehland LA, Hill HH. Improved momentum-transfer theory for ion mobility. 1. Derivation of the fundamental equation. Anal Chem. 2012;84:9782–91.
29. Stow SM, Causon TJ, Zheng X, Kurulugama RT, Mairinger T, May JC, Rennie EE, Baker ES, Smith RD, McLean JA, Hann S, Fjeldsted JC. An interlaboratory evaluation of drift tube ion mobility–mass spectrometry collision cross section measurements. Anal Chem. 2017;89:9048–55.
30. Causon TJ, Hann S. Uncertainty estimations for collision cross section determination via uniform field drift tube-ion mobility-mass spectrometry. J Am Soc Mass Spectrom. 2020;31:2102–10
31. Bush MF, Hall Z, Giles K, Hoyes J, Robinson CV, Ruotolo BT. Collision cross sections of proteins and their complexes: A calibration framework and database for gas-phase structural biology. Anal Chem. 2010;82:9557–65.
32. Valentine SJ, Clemmer DE. Treatise on the measurement of molecular masses with ion mobility spectrometry. Anal Chem. 2009;81:5876–80.
33. Wojcik R, Nagy G, Attah IK, Webb IK, Garimella SVB, Weitz KK, Hollerbach A, Monroe ME, Ligare MR, Nielson FF, Norheim RV, Renslow RS, Metz TO, Ibrahim YM, Smith RD. SLIM ultra-high resolution ion mobility spectrometry separations of isotopologues and isotopomers reveal mobility shifts due to mass distribution changes. Anal Chem. 2019;91:11952–62.
34. Viehland LA, Lin SL, Mason EA. Kinetic theory of drift-tube experiments with polyatomic species. Chem Phys. 1981;54:341–64.
35. Viehland LA. Mobilities of isotopic ions in gases. Int J Ion Mobil Spectrom. 2016;19:11–4.
36. Kirk AT, Raddatz CR, Zimmermann S. Separation of isotopologues in ultra-high-resolution ion mobility spectrometry. Anal Chem. 2017;89:1509–15.
37. Schaefer C, Kirk AT, Allers M, Zimmermann S. Ion mobility shift of isotopologues in a high kinetic energy ion mobility spectrometer (HiKE-IMS) at elevated effective temperatures. J Am Soc Mass Spectrom. 2020;31:2093–101.
38. Viehland LA. Mobilities of mixtures of ion isotopes in gas mixtures. Int J Ion Mobil Spectrom. 2016;19:1–10.
39. Asbury GR, Hill HH. Using different drift gases to change separation factors (α) in ion mobility spectrometry. Anal Chem. 2000;72:580–4.
40. Kurulugama RT, Darland E, Kuhlmann F, Stafford G, Fjeldsted J. Evaluation of drift gas selection in complex sample analyses using a high performance drift tube ion mobility-QTOF mass spectrometer. Analyst. 2015;140:6834–44.
41. Morris CB, May JC, Leaptrot KL, McLean JA. Evaluating separation selectivity and collision cross section measurement reproducibility in helium, nitrogen, argon, and carbon dioxide drift gases for drift tube ion mobility–mass spectrometry. J Am Soc Mass Spectrom. 2019;30:1059–68.
42. Fernández-Maestre R, Wu C, Hill Jr HH. Buffer gas modifiers effect resolution in ion mobility spectrometry through selective ion-molecule clustering reactions. Rapid Commun Mass Spectrom. 2012;26:2211–23.
43. Waraksa E, Perycz U, Namieśnik J, Sillanpää M, Dymerski T, Wójtowicz M, Puton J. Dopants and gas modifiers in ion mobility spectrometry. TrAC, Trends Anal Chem. 2016;82:237–49.
44. Kirk AT, Bakes K, Zimmermann S. A universal relationship between optimum drift voltage and resolving power. Int J Ion Mobil Spectrom. 2017;20:105–9.
45. Dodds JN, May JC, McLean JA. Correlating resolving power, resolution, and collision cross section: Unifying cross-platform assessment of separation efficiency in ion mobility spectrometry. Anal Chem. 2017;89:12176–84.
46. Langejuergen J, Allers M, Oermann J, Kirk A, Zimmermann S. High kinetic energy ion mobility spectrometer: Quantitative analysis of gas mixtures with ion mobility spectrometry. Anal Chem. 2014;86:7023–32.
47. Shvartsburg AA, Li F, Tang K, Smith RD, High-resolution field asymmetric waveform ion mobility spectrometry using new planar geometry analyzers. Anal Chem. 2006;78:3706–14.
48. Bohnhorst A, Kirk AT, Berger M, Zimmermann S. Fast orthogonal separation by superposition of time of flight and field asymmetric ion mobility spectrometry. Anal Chem. 2018;90:1114–21.
49. Siems WF, Viehland LA, Hill HH. Correcting the fundamental ion mobility equation for field effects. Analyst. 2016;141:6396–407.
50. Mesleh MF, Hunter JM, Shvartsburg AA, Schatz GC, Jarrold MF. Structural information from ion mobility measurements: Effects of the long-range potential. J Phys Chem. 1996;100:16082–6.

51. Viehland LA. Ion–atom interaction potentials and transport properties. Comput Phys Commun. 2001;142:7–13.
52. Bleiholder C, Wyttenbach T, Bowers MT. A novel projection approximation algorithm for the fast and accurate computation of molecular collision cross sections (I). Method. Int J Mass spectrom. 2011;308:1–10.
53. Larriba C, Hogan CJ. Ion mobilities in diatomic gases: Measurement versus prediction with non-specular scattering models. J Phys Chem A. 2013;117:3887–901.
54. Zanotto L, Heerdt G, Souza PCT, Araujo G, Skaf MS. High performance collision cross section calculation—HPCCS. J Comput Chem. 2018;39:1675–81.
55. Ieritano C, Crouse J, Campbell JL, Hopkins WS. A parallelized molecular collision cross section package with optimized accuracy and efficiency. Analyst. 2019;144:1660–70.
56. Giles K, Pringle SD, Worthington KR, Little D, Wildgoose JL, Bateman RH. Applications of a travelling wave-based radio-frequency-only stacked ring ion guide. Rapid Commun Mass Spectrom. 2004;18:2401–14.
57. Giles K, Williams JP, Campuzano I. Enhancements in travelling wave ion mobility resolution. Rapid Commun Mass Spectrom. 2011;25:1559–66.
58. Shvartsburg AA, Smith RD. Fundamentals of traveling wave ion mobility spectrometry. Anal Chem. 2008;80:9689–99.
59. Smith DP, Knapman TW, Campuzano I, Malham RW, Berryman JT, Radford SE, Ashcroft AE. Deciphering drift time measurements from travelling wave ion mobility spectrometry-mass spectrometry studies. Eur J Mass Spectrom. 2009;15:113–30.
60. Forsythe JG, Petrov AS, Walker CA, Allen SJ, Pellissier JS, Bush MF, Hud NV, Fernández FM. Collision cross section calibrants for negative ion mode traveling wave ion mobility-mass spectrometry. Analyst. 2015;140:6853–61.
61. Haler JRN, Kune C, Massonnet P, Comby-Zerbino C, Jordens J, Honing M, Mengerink Y, Far J, De Pauw E. Comprehensive ion mobility calibration: Poly(ethylene oxide) polymer calibrants and general strategies. Anal Chem. 2017;89:12076–86.
62. Richardson K, Langridge D, Giles K. Fundamentals of travelling wave ion mobility revisited: I. Smoothly moving waves. Int J Mass spectrom. 2018;428:71–80.
63. Giddings JC. Maximum number of components resolvable by gel filtration and other elution chromatographic methods. Anal Chem. 1967;39:1027–8.
64. Davis JM, Giddings JC. Statistical theory of component overlap in multicomponent chromatograms. Anal Chem. 1983;55:418–24.
65. Causon TJ, Hann S. Theoretical evaluation of peak capacity improvements by use of liquid chromatography combined with drift tube ion mobility-mass spectrometry. J Chromatogr A. 2015;1416:47–56.
66. Grushka E. Chromatographic peak capacity and the factors influencing it. Anal Chem. 1970;42:1142–7.
67. Neue UD. Peak capacity in unidimensional chromatography. J Chromatogr A. 2008;1184:107–30.
68. Horvath CG, Lipsky SR. Peak capacity in chromatography. Anal Chem. 1967;39:1893.
69. Kirk AT, Zimmermann S. An analytical model for the optimum drift voltage of drift tube ion mobility spectrometers with respect to resolving power and detection limits. Int J Ion Mobil Spectrom. 2015;18:129–35.
70. Gaš B, Štědrý M, Kenndler E. Peak broadening in capillary zone electrophoresis. Electrophoresis. 1997;18:2123–33.
71. Zwillinger D, Moll V, Gradshteyn IS, Ryzhik IM. Table of integrals, series, and products. 8th ed. Boston: Academic Press; 2014.
72. Potts LW, Carr PW. Approximate and exact equations for peak capacity in isocratic high-pressure liquid chromatography. Anal Chem. 2011;83:7614–5.

SUPPORTING INFORMATION

Additional supporting information may be found online in the Supporting Information section at the end of the article.

How to cite this article: Grabarics M, Lettow M, Kirk AT, von Helden G, Causon TJ, Pagel K. Plate-height model of ion mobility-mass spectrometry: Part 2—Peak-to-peak resolution and peak capacity. J Sep Sci. 2021;44:2798–2813. https://doi.org/10.1002/jssc.202100201